Consistent formulation of solid dissipative effects in stability analysis of flow past a deformable solid

D. Giribabu and V. Shankar*
Department of Chemical Engineering, Indian Institute of Technology, Kanpur 208016, India
(Received 24 February 2016; published 21 July 2016)

The linear stability of plane Couette flow past a deformable solid is analyzed in the creeping-flow limit with an objective towards elucidating the consequences of employing two widely different formulations for the dissipative stresses in the deformable solid. One of the formulations postulates that the dissipative stress is proportional to the strain-rate tensor based on the left Cauchy-Green tensor, while in the other the dissipative stress in the solid is proportional to the rate-of-deformation tensor. However, it is well known in continuum mechanics that the rate-of-deformation tensor obeys the fundamental principle of material-frame indifference while the strain-rate-tensor formulation does not and hence it is more appropriate to employ the rate-of-deformation tensor in the description of dissipative stresses in deformable solids. In this work we consider the specific context of stability of plane Couette flow past a deformable solid and demonstrate that the results concerning the stability of the system from both models differ drastically. In the rate-of-deformation formulation for the dissipative stress, there is a range of solid-fluid thickness ratios (between 1.21 and 1.46) wherein the system is always stable for nonzero values of solid viscosity, unlike the strain-rate-tensor formulation wherein the system is unstable at all values of solid thickness. Further, for a solid-fluid thickness ratio less than 1, incorporation of dissipative effects in the solid using the rate-of-deformation formulation shows that the flow is more unstable compared to a purely elastic neo-Hookean solid, while for strain-rate-tensor formulation the flow is stabilized with an increase in viscosity of the solid. Using the fundamentally correct dissipative stress formulation, we also address the stability of pressure-driven flow in a deformable channel, wherein previous work carried out for an elastic neo-Hookean solid has shown that only the short-wave instability (driven by the first normal stress difference in the solid) exists while the finite-wave instability is absent in the creeping-flow limit. Using a consistent formulation for viscous stresses in the solid, we show that the short-wave instability is completely stabilized beyond a critical viscosity of the solid. Thus the present study clearly demonstrates the importance of consistent modeling of dissipative effects in the solid in order to accurately predict the stability of fluid flow past deformable solid surfaces.

DOI: 10.1103/PhysRevFluids.1.033602

I. INTRODUCTION

Fluid flow past soft deformable solid surfaces has been studied theoretically as well as experimentally in the literature because of its relevance to technological applications and to biological flows. In microfluidic devices [1–3], because of their submillimeter dimensions, the flow usually happens to be laminar and it requires a very high pressure drop to pump the fluid, resulting in poor transport rates. Mixing in such devices is usually enhanced by either active or passive manipulation of the flow [4]. Active methods such as electrokinetic flows [5] and surface modification [3] have issues of moving external parts and cost of energy. Passive methods such as flow focusing, split recombination, deformable walls [6–11], and soft-elastomer coatings [12] can potentially provide an alternative because of their nonintrusive nature and ease of fabrication. For the past two decades,

*Corresponding author: vshankar@iitk.ac.in

flow past deformable solid surfaces has generated immense interest because of drag reduction mainly in marine and aerospace applications, but these are external flows [13]. Research in internal flows in deformable tubes arguably started with the experimental work of Krindel and Silberberg [14]. They observed a higher drag force and pressure drop for flow through a gel-coated deformable tube. Recent experiments [15] have shown fivefold enhancement of mixing and a significant reduction in the transition Reynolds number in a channel flow with a deformable wall and have further shown [16] that a turbulentlike state is achieved in a microchannel (with soft walls) at a Reynolds number around 250. These experimental results have motivated several theoretical studies in flow through deformable channels and tubes, which will have implications in the design and function of microfluidic devices fabricated using deformable elastomers.

Kumaran *et al.* [6] first analyzed the stability plane Couette flow past a deformable solid in the zero-Re (creeping-flow) limit and showed that the flow is unstable in this limit. The dominant wave number for this instability is $O(1)$ and this is referred to as the finite-wave instability (or the viscous mode), which exists even for a solid-fluid thickness ratio $H \gg 1$. With the inclusion of viscous dissipation η_r in the solid, the finite-wave instability exists only for $H > \sqrt{\eta_r}$. Later, Muralikrishnan and Kumaran [7,17] demonstrated experimentally the onset of finite-wave instability in Couette flow. Gkanis and Kumar [8] argued that for the strains that are involved in the experiments, it is appropriate to use the frame-invariant neo-Hookean model to describe the deformation in the solid layer. In addition to the finite-wave-number instability [6], Gkanis and Kumar also predicted a new short-wave instability that arises because of the first normal stress difference in the base state of the neo-Hookean solid. The finite-wave-number instability is the most unstable mode when the ratio of solid to fluid thickness is large (greater than 1), while the short-wave mode is critical for smaller values of solid to fluid thickness ratios. Eggert and Kumar [18] carried out experiments on Couette flow to probe the postinstability scenario and found that the instability is subcritical in nature, which is in qualitative agreement with the theoretical predictions of Shankar and Kumaran [19]. Previous experimental studies [17,20,21] have typically considered poly(dimethyl)siloxane or polyacrylamide gels for which the loss modulus G'' is comparable to the storage modulus G', which implies that solid viscosity $\eta_s = \frac{G''}{\omega}$ (ω being the frequency) could play an important role in the stability of fluid flow past deformable solid surfaces. Hence, it is important to accurately model the dissipation in the solid in order to validate theoretical predictions with experimental observations. In the literature, viscous dissipation in a deformable solid has been modeled in two drastically different ways. One formulation uses the strain-rate tensor $\dot{\mathbf{E}}_{\text{left}}$ [22,23] based on the left Cauchy-Green deformation tensor, while the other uses the rate-of-deformation tensor $\mathbf{D}$ [9,10]. Chokshi and Kumaran [22] considered the strain-rate tensor to model dissipation in the solid and showed that instability exists for all values of solid thickness. In the regime when $\sqrt{\eta_r}/H < 1$, viscosity stabilizes the flow, while for $\sqrt{\eta_r}/H > 1$, viscosity destabilizes the flow. In contrast, in the linear elastic solid, viscosity always stabilizes the flow. Gaurav and Shankar [9] used a rate-of-deformation tensor for dissipation in the channel flow and showed that inclusion of dissipation always stabilizes the flow at high Reynolds number but they did not examine the role of dissipation in the creeping-flow limit in their work. Destrade *et al.* [24] showed that the strain-rate tensor is not the appropriate choice for incorporating viscous stresses in the solid, as this led to an unphysical kink in the wave formation and suggested the use of the rate-of-deformation tensor.

In the present work we demonstrate the consequences of using the two different formulations for the dissipative viscous stress in the solid in the context of plane Couette and plane Poiseuille flows past a deformable solid layer. The rest of the paper is organized as follows. Section II describes the configuration considered and the constitutive equations for both the fluid and solid used in this work. Linear stability analysis is carried out for the plane Couette flow and the corresponding linearized equations are given in Sec. III. Section IV discusses the results obtained from both the solid viscous dissipation formulations and their effect on the flow stability for plane Couette flow. In the case of pressure-driven channel flow, the consequences of incorporating the rate-of-deformation tensor for the viscous stress on the flow stability are discussed. The major findings of the present study are summarized in Sec. V.

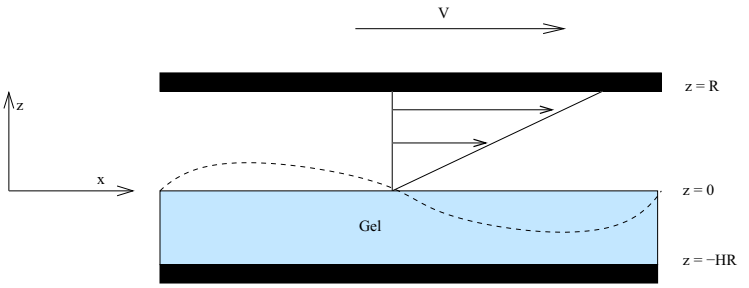

FIG. 1. Schematic representation of plane Couette flow past a deformable solid and the (dimensional) coordinate system used.

II. PROBLEM FORMULATION

We first consider the plane Couette flow past a deformable solid layer (Fig. 1) in the creeping-flow regime. The top plate (at $z = 1$) moves with velocity V and the bottom plate (at $z = -HR$) is held stationary. The deformable solid of shear modulus G occupies the region $0 > z > -HR$ and is rigidly bonded to the stationary bottom plate. A Newtonian fluid of density ρ_f and viscosity η_f occupies the region $0 < z < R$ between the deformable solid and top plate. The governing equations of the fluid and solid are nondimensionalized by scaling the velocities with $\frac{GR}{\eta_f}$, distances with R, time with $\frac{\eta_f}{G}$, solid viscosity with η_f, and pressure and stresses with G (shear modulus of the solid). The nondimensional governing equations of mass and momentum for the fluid in the creeping-flow limit are given by

$$\nabla \cdot \mathbf{v} = 0, \quad \nabla \cdot \boldsymbol{\tau} = 0, \tag{1}$$

where $\mathbf{v}$ is the velocity and $\boldsymbol{\tau}$ is the shear stress tensor in the fluid

$$\boldsymbol{\tau} = -p_f \mathbf{I} + [\nabla \mathbf{v} + (\nabla \mathbf{v})^T]. \tag{2}$$

The deformable solid is modeled as an incompressible neo-Hookean elastic solid with dissipation [8,9,22,25,26]. In the Lagrangian description, the particle motion in the solid is described by

$$\mathbf{x}(\mathbf{X},t) = \mathbf{X} + \mathbf{u}(\mathbf{X},t), \tag{3}$$

where $\mathbf{X}$ is the reference position of a material particle at time $t = 0$, $\mathbf{x}$ is the current position of the particle at any time t, and $\mathbf{u}$ is the displacement vector of the particle. The incompressibility condition in the solid is expressed as [25]

$$\det(\mathbf{F}) = 1, \quad \mathbf{F} = \frac{\partial \mathbf{x}}{\partial \mathbf{X}}, \tag{4}$$

where $\mathbf{F}$ is the Lagrangian deformation gradient tensor in the solid. Many polymer gels and soft elastomers also exhibit dissipative behavior during deformation and hence it is necessary to include this as well in the stress tensor. The shear stress in the solid thus is comprised of both elastic and dissipative parts as considered in previous studies [27]:

$$\boldsymbol{\sigma} = \boldsymbol{\sigma}^E + \boldsymbol{\sigma}^D, \tag{5}$$

$$\boldsymbol{\sigma}^E = -p_s \mathbf{I} + 2G\mathbf{E}_{\text{left}}, \quad \mathbf{E}_{\text{left}} = \tfrac{1}{2}(\mathbf{F} \cdot \mathbf{F}^T - \mathbf{I}), \tag{6}$$

where $\boldsymbol{\sigma}$ is the Cauchy stress tensor and $\mathbf{E}_{\text{left}}$ is the Lagrangian strain tensor based on the left Cauchy-Green deformation tensor $\mathbf{F} \cdot \mathbf{F}^T$. It must be noted that in traditional continuum mechanics [25,26], the Lagrangian strain tensor $\mathbf{E} = \frac{1}{2}(\mathbf{F}^T \cdot \mathbf{F} - \mathbf{I})$ is defined based on the right Cauchy-Green deformation tensor. In order to distinguish the two strain tensors, we use the subscript left to indicate

the strain tensor based on the left Cauchy-Green deformation tensor. There have been two widely different formulations that were employed in earlier studies to model the dissipative contribution $\boldsymbol{\sigma}^D$ to the stress tensor in the solid. In one approach [27,28], the dissipative part of stress tensor is given by

$$\boldsymbol{\sigma}^D = 2\eta_s \mathbf{D}, \quad \mathbf{D} = \tfrac{1}{2}(\mathbf{L} + \mathbf{L}^T), \quad \mathbf{L} = \dot{\mathbf{F}} \cdot \mathbf{F}^{-1}, \tag{7}$$

where $\mathbf{D}$ is the rate-of-deformation tensor and $\mathbf{L}$ is the spatial velocity gradient tensor [25,26].

In another approach [22,23] the dissipative part is considered as

$$\boldsymbol{\sigma}^D = 2\eta_s \dot{\mathbf{E}}_{\text{left}}, \quad \dot{\mathbf{E}}_{\text{left}} = \frac{1}{2}\left[\frac{\partial}{\partial t}(\mathbf{F} \cdot \mathbf{F}^T - \mathbf{I})\right]_{\mathbf{X}}, \tag{8}$$

where $\dot{\mathbf{E}}_{\text{left}}$ is the strain-rate tensor obtained by taking the material time derivative of the strain tensor $\mathbf{E}_{\text{left}}$. While considering constitutive relations for a solid, especially at finite deformations, the relation for the Cauchy stress tensor $\boldsymbol{\sigma}$ must obey the principle of material frame indifference [25]. In a neo-Hookean solid, the elastic part of the stress is proportional to $\mathbf{F} \cdot \mathbf{F}^T$, which is frame invariant. It is a proven fact in continuum mechanics that the rate-of-deformation tensor $\mathbf{D}$ is frame indifferent, while the strain-rate tensor $\dot{\mathbf{E}}_{\text{left}}$ is not [25,29]. Hence it is not appropriate to describe the dissipative stress in the solid using $\dot{\mathbf{E}}_{\text{left}}$. Recent studies [24,30] have also emphasized that the strain-rate tensor is not appropriate for incorporating viscous dissipative effects, as it yields unphysical results in the context of wave formation in prestressed viscoelastic solids [31]. In this work, we employ both formulations and demonstrate how the use of the (incorrect) strain-rate formulation for the dissipative stress leads to results that are drastically different from the rate-of-deformation formulation. The equation of motion in the solid is given as

$$\boldsymbol{\nabla}_{\mathbf{X}} \cdot \mathbf{P} = 0, \quad \mathbf{P} = \mathbf{F}^{-1} \cdot \boldsymbol{\sigma}, \tag{9}$$

where $\mathbf{P}$ is the first Piola-Kirchhoff stress tensor.

The nondimensional base state velocity for plane Couette flow is of the form

$$v_x = \Gamma z, \tag{10}$$

where $\Gamma = V\eta_f / GR$ is the nondimensional strain rate in the base flow. The base state deformation of the solid is given as

$$\mathbf{x} = (x_1, x_2, x_3) = [X_1 + \Gamma(X_3 + H), X_2, X_3]. \tag{11}$$

The Cauchy stress in the neo-Hookean solid exhibits first the normal stress difference ($\sigma_{xx} - \sigma_{zz} = \Gamma^2$) in the base state, which gives rise to short-wave instability [8], but this feature is absent in the linear elastic solid [6].

III. LINEAR STABILITY ANALYSIS

The temporal stability of plane Couette flow is analyzed by imposing small perturbations to the base state and the governing equations are then linearized. In this study, we consider two-dimensional perturbations of the general form

$$f' = \tilde{f}(z) \exp(ikx + st), \tag{12}$$

where $\tilde{f}(z)$ is the amplitude of the disturbance, k is the wave number, which is a real quantity, and s is the growth rate, which is a complex quantity in a temporal stability analysis. If $\text{Re}[s] < 0$ then the flow is stable, if $\text{Re}[s] > 0$ the flow is unstable, and if $\text{Re}[s] = 0$ the flow is neutrally stable. Infinitesimal perturbations are imposed on the velocity, pressure, and displacement in the governing equations and boundary conditions. After neglecting the nonlinear terms, the linearized governing

equations are of the form

$$d_z\tilde{v}_z + ik\tilde{v}_x = 0, \tag{13}$$

$$-ik\tilde{p}_f + \left(d_z^2 - k^2\right)\tilde{v}_x = 0, \tag{14}$$

$$-d_z\tilde{p}_f + \left(d_z^2 - k^2\right)\tilde{v}_z = 0. \tag{15}$$

The linearized governing equations for the solid (using the rate of deformation tensor $\mathbf{D}$ for dissipation) are given by

$$d_{X_3}\tilde{x}_3 + ik\tilde{x}_1 - ik\Gamma\tilde{x}_3 = 0, \tag{16}$$

$$-ik\tilde{p}_s + \left(d_{X_3}^2 - k^2\right)\tilde{x}_1 + s\eta_r\left[\left(d_{X_3}^2 - k^2\right)\tilde{x}_1 - \Gamma^2k^2\tilde{x}_1 - 2ik\Gamma d_{X_3}\tilde{x}_1\right] = 0, \tag{17}$$

$$ik\Gamma\tilde{p}_s - d_{X_3}\tilde{p}_s + \left(d_{X_3}^2 - k^2\right)\tilde{x}_3 + s\eta_r\left[\left(d_{X_3}^2 - k^2\right)\tilde{x}_3 - \Gamma^2k^2\tilde{x}_3 - 2ik\Gamma d_{X_3}\tilde{x}_3\right] = 0, \tag{18}$$

where $\eta_r = \frac{\eta_s}{\eta_f}$ is the solid to fluid viscosity ratio. The corresponding linearized governing equations for the solid when the strain-rate tensor is employed for the dissipative stress are provided in the Appendix. The linearized boundary conditions at the fluid-solid interface are

$$\tilde{v}_x + \Gamma\tilde{x}_3 - s\tilde{x}_1 = 0, \tag{19}$$

$$\tilde{v}_z - s\tilde{x}_3 = 0, \tag{20}$$

$$ik(1-\Gamma^2)\tilde{x}_3 + \Gamma d_{X3}\tilde{x}_3 + d_{X3}\tilde{x}_1 + s\eta_r[ik\tilde{x}_3 + d_{X3}\tilde{x}_1 - ik\Gamma\tilde{x}_1] - d_z\tilde{v}_x - ik\tilde{v}_z = 0, \tag{21}$$

$$\tilde{p}_s - 2(1+s\eta_r)d_{X3}\tilde{x}_3 + 2\eta_r ik\Gamma s\tilde{x}_3 - \tilde{p}_f + 2d_z\tilde{v}_z - k^2\gamma\tilde{x}_3 = 0. \tag{22}$$

The boundary conditions at the top and bottom rigid plates are

$$\tilde{x}_3 = 0, \quad \tilde{x}_1 = 0 \quad \text{at } z = -H, \tag{23}$$

$$\tilde{v}_z = 0, \quad \tilde{v}_x = 0 \quad \text{at } z = 1. \tag{24}$$

The linearized equations for the fluid (13)–(15) and solid (16)–(18) are combined to form a single fourth-order equation for each medium and are solved analytically for the respective general solutions, which are given by

$$\tilde{v}_z(z) = A_1e^{-kz} + A_2ze^{-kz} + A_3e^{kz} + A_4ze^{kz}, \tag{25}$$

$$\tilde{x}_3(z) = B_1e^{m_1} + B_2e^{(-1+i\Gamma)kz} + B_3e^{m_2} + B_4e^{(1+i\Gamma)kz}, \tag{26}$$

where $m_1 = [(i\eta_r\Gamma ks + \sqrt{k^2 + 2\eta_rk^2s + \eta_r\Gamma^2k^2s + \eta_r^2k^2s^2})z]/(1+\eta_rs)$ and $m_2 = [(i\eta_r\Gamma ks - \sqrt{k^2 + 2\eta_rk^2s + \eta_r\Gamma^2k^2s + \eta_r^2k^2s^2})z]/(1+\eta_rs)$. The eigenfunctions are substituted into the boundary conditions (19)–(22) to construct a matrix of the form

$$\mathbf{Ma} = 0, \tag{27}$$

where $\mathbf{M}$ is an 8×8 matrix and the vector $\mathbf{a} = [A_1, A_2, A_3, A_4, B_1, B_2, B_3, B_4]^T$. The determinant of the matrix $\mathbf{M}$ is set to zero to find the nontrivial solution, which yields the characteristic equation. This equation is solved for the growth rate s by specifying the parameters H, Γ, η_r, and k. The characteristic equation is a transcendental equation for growth rate s for nonzero values of the viscosity ratio η_r and hence it has to be solved numerically by a Newton-Raphson iteration procedure. When $\eta_r = 0$, the characteristic equation is quadratic and this allows for analytical solutions for

growth rate s. A spectral method [32] is also implemented to solve the fourth-order differential equations for the fluid and solid with the boundary conditions for the growth rate s as an eigenvalue, since this method provides all the eigenvalues without the need for an initial guess. The results of the spectral method serve as an initial guess for the Newton-Raphson method to determine the growth rate. From this we plot the neutral stability curves in the Γ-k parametric space. The minimum value of Γ in this curve is called the critical strain rate Γ_c since it is the lowest Γ required to make the flow just unstable for a specified set of parameters H and η_r.

IV. RESULTS

A. Couette flow

First, we recapitulate the results obtained in earlier studies [6,8] for a pure elastic solid, which is then followed by a discussion of the results obtained in this work focusing on the effect of solid viscosity using the two different formulations for dissipation in the solid. Using the linear elastic solid model, it was demonstrated [6] that the plane Couette flow past a deformable solid becomes unstable when Γ increases beyond a certain critical value. For solid thickness $H \sim O(1)$, Γ_c is $O(1)$ and k_c (the corresponding critical wave number) is also $O(1)$, indicating that the instability is a finite wavelength instability. For $H \gg 1$, $\Gamma_c \propto 1/H$ and $k_c \sim 1/H$, suggesting that the most unstable mode becomes much longer. Even for a neo-Hookean solid [8], it was shown that for $H \gg 1$, the results are very similar to that obtained from the linear elastic model; however, for $H \leqslant 1$, a new unstable mode arises at short wavelengths due to the first normal stress difference in the base state of the neo-Hookean solid. This physical effect is absent in the linear elastic model and hence this instability was not predicted using linear elastic model [6].

In our work, for the case of a purely elastic neo-Hookean solid ($\eta_r = 0$), we have verified that the results are the same as reported by Gkanis and Kumar [8] and the corresponding neutral curves at different thickness can be seen in Figs. 2(a)–2(d). When viscous dissipation in the solid is included, it can be taken in two forms, using either $\dot{\mathbf{E}}_{\text{left}}$ or $\mathbf{D}$. The relation between $\dot{\mathbf{E}}_{\text{left}}$ and $\mathbf{D}$ is given by $\dot{\mathbf{E}}_{\text{left}} = \frac{1}{2}(\mathbf{L}\cdot\mathbf{F}\cdot\mathbf{F}^T + \mathbf{F}\cdot\mathbf{F}^T\cdot\mathbf{L}^T)$. For infinitesimal strains, $\mathbf{F}^T \simeq \mathbf{F} \approx \mathbf{I}$ and hence $\dot{\mathbf{E}}_{\text{left}} \approx \mathbf{D}$. However, for finite strains, this does not hold and in general $\dot{\mathbf{E}}_{\text{left}}$ and $\mathbf{D}$ are very different. For this reason, the momentum balance equations for the solid with these two models for dissipation are vastly different. This leads to drastically different results for different formulations for the viscosity. Now the question arises as to which formulation is the consistent one for viscous dissipation in solids. To answer that question, we first recall the previous work of Chokshi and Kumaran [22], where they considered the strain-rate tensor for the viscous part, which is a symmetric tensor. However, this is not a consistent formulation for viscoelastic solids as the strain-rate tensor is not frame invariant (see Ref. [25], p. 403 and Ref. [29], pp. 105–106). The rate-of-deformation tensor does not violate the principle of material frame invariance and hence it is appropriate to use the rate-of-deformation tensor $\mathbf{D}$ for the viscous part in the Cauchy stress tensor. In the recent work of Destrade *et al.* [24], the addition of the strain-rate tensor to the first Piola-Kirchhoff stress tensor gave rise to waves with a sharp kink on a soft solid, which is unphysical, and this was attributed to the use of the strain-rate tensor to model dissipative effects in the solid.

To reconcile the issue of material-frame indifference, Destrade *et al.* [24] suggested the use of the rate-of-deformation tensor $\mathbf{D}$, which resulted in the removal of an unphysical kink and gave rise to a gentle slope in the waves. The work of Destrade *et al.* is on wave propagation in the soft solid alone, but the present work is concerned with the stability of the coupled fluid-solid system. Here, as we demonstrate below, we find major differences in the results obtained using different viscous formulation terms. In the previous work of Chokshi and Kumaran [22], they used the strain-rate tensor for the viscous term, which predicts instability at all solid thicknesses. However, as discussed above, this is not the proper formulation for modeling dissipative stresses in the solid. When the rate of deformation tensor is considered, the results are significantly different when compared to the results obtained using the strain-rate tensor. First we demonstrate the differences that arise in

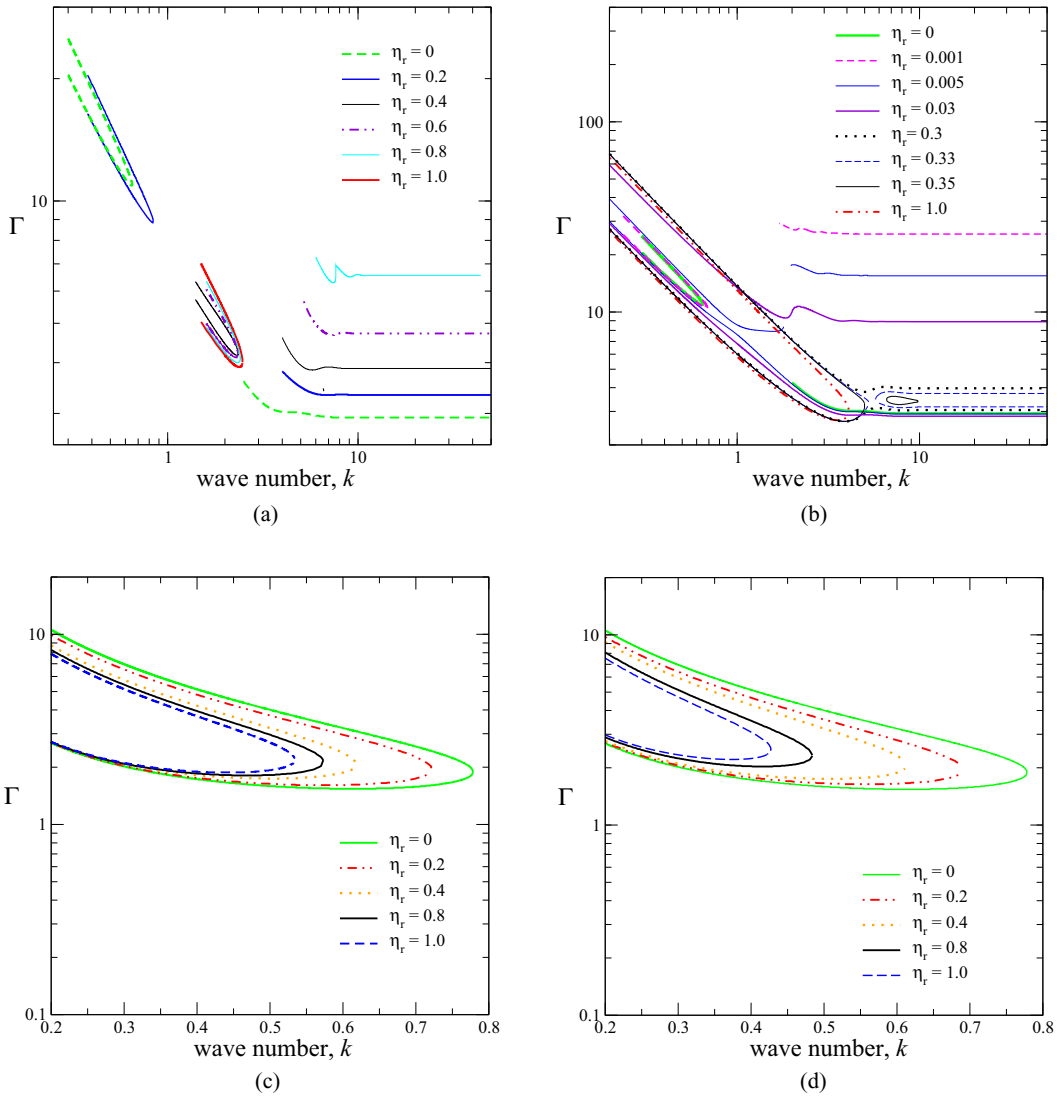

FIG. 2. Neutral stability curves in the Γ-k plane for the interfacial instability for two different values of solid thickness H and at different values of η_r obtained from two formulations for dissipation. (a) and (b) Neutral curves for both possible modes of instability and (c) and (d) only the finite-wave number mode is shown as the short-wave mode is not observed for the range of Γ illustrated in this figure. (a) $H = 0.5$, strain-rate formulation; (b) $H = 0.5$, rate-of-deformation formulation; (c) $H = 2$, strain-rate formulation; and (d) $H = 2$, rate-of-deformation formulation.

the neutral stability curves in the Γ-k plane both at low and high H. In particular, at low H, the behaviors of the neutral curves obtained from the two formulations are significantly different. At low H, inclusion of viscosity using the strain-rate-tensor formulation has contrasting effects on finite-wave and short-wave modes. An increase in viscosity η_r stabilizes the short-wave mode and destabilizes the finite-wave mode, and at $\eta_r = 1$, the short-wave mode gets fully stabilized, which can be seen in Fig. 2(a). For the same case, when viscous dissipation in the solid is modeled using the rate-of-deformation tensor, the results show interesting behavior at low H. There exists an upper branch for the short-wave mode (beyond which there is no instability) even for the smallest value of

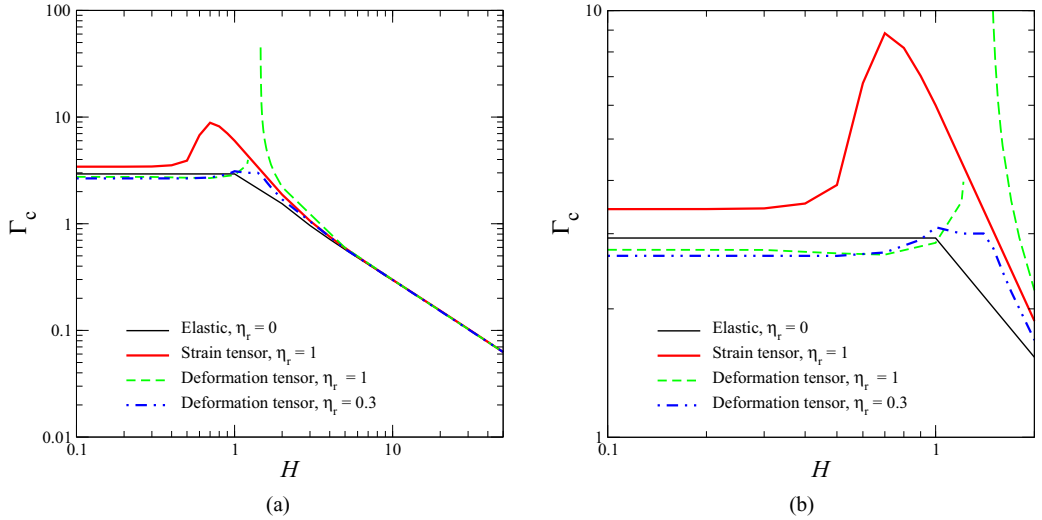

FIG. 3. Plane Couette flow past a deformable solid. (a) Critical strain rate as a function of thickness H for different η_r. (b) Zoomed in view of (a) for smaller values of H.

$\eta_r = 10^{-7}$. This feature is absent in the strain-rate-tensor formulation. With an increase in viscosity, first the finite-wave mode splits into two branches and then the lower branch of the short-wave mode merges with the lower branch of the finite-wave mode and the upper branch of the short-wave mode merges with the upper branch of the finite-wave mode until $\eta_r = 0.33$. After $\eta_r = 0.33$, both the short-wave and finite-wave modes separate out again and the short-wave neutral curve becomes a closed curve. A further increase in the viscosity makes the closed short-wave neutral curve shrink and eventually disappear and the short-wave mode gets totally stabilized [Fig. 2(b)]. Thus, only the finite-wave mode remains after $\eta_r = 0.35$, but the critical strain rate obtained for the finite-wave mode is lower than the critical strain rate obtained for a pure elastic solid. However, this is not the case with the strain-rate tensor. At high H, both models predict similar behavior for the neutral stability curves, which are shown in Figs. 2(c) and 2(d), but there is a difference in the critical strain rate Γ_c until $H = 5$. For $H > 5$, both models predict nearly the same critical strain-rate values. The critical strain rate Γ_c is plotted as a function of H for specified values of η_r in Fig. 3(a). For both formulations, the critical Γ_c is independent of H for $H \ll 1$ for the short-wave instability. The reason why this happens is explained by noting that for the short-wave instability, the length scale over which the eigenfunctions are in solid decay is proportional to k^{-1} and hence the solid layer thickness H does not play any role.

For the strain-rate-tensor formulation, inclusion of viscous effects always stabilizes the flow at all thicknesses for $\eta_r = 1$ when compared to a purely elastic solid. The results obtained using the rate-of-deformation tensor, in contrast, exhibit the opposite behavior at both low and high H, as shown in Fig. 3(a). At low H, inclusion of viscosity destabilizes the flow because of modes merging and separating for $\eta_r = 1$, as shown in Fig. 2(b), and viscous dissipation stabilizes the flow at high H where the finite-wave mode is critical for instability, as shown in Fig. 2(d). In Fig. 3(a) there is a break in the unstable zone between thicknesses $H = 1.21$ and $H = 1.46$, implying that at these thickness values, no matter how high Γ is, there is no instability, as shown in Figs. 3(a) and 3(b). The break in the unstable zone does not exist for low η_r as demonstrated for the case of $\eta_r = 0.3$. For linear elastic solids, Kumaran *et al.* [6] showed that for the finite-wave mode, Γ_c scales as $(H - \sqrt{\eta_r})^{-1}$ for $H > 1$. For neo-Hookean solids, the corresponding scalings are different for the two dissipative formulations. The results obtained using the strain-rate tensor show the scaling of the critical strain rate as $\Gamma_c \propto H^{-1}$ for $\sqrt{\eta_r}/H < 1$ and for the case of $\sqrt{\eta_r}/H > 1$, $\Gamma_c \propto H^{-1/2}$, which is shown in Fig. 4(a) (which is the same as that reported in Ref. [22]). At sufficiently high

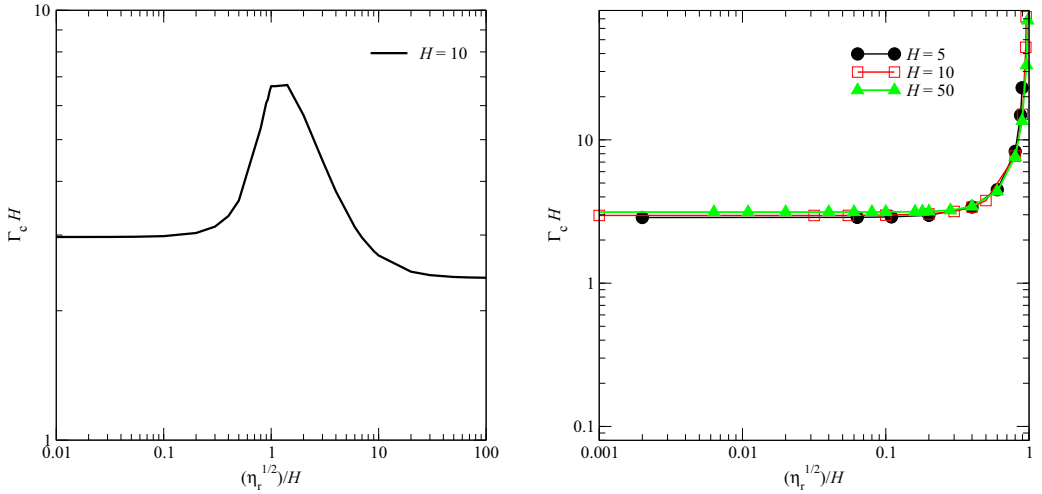

FIG. 4. Plane Couette flow past a deformable solid. Scaling of Γ_c with η_r for $H \gg 1$ is shown for the two different formulations of viscous effects in the solid: (a) strain-rate-tensor formulation and (b) rate-of-deformation tensor formulation.

values of $\sqrt{\eta_r}/H$, Γ_c once again scales as H^{-1}. The results obtained using the rate-of-deformation tensor do not have two different scalings as shown by strain-rate tensor but follow a scaling similar to that found in the linear elastic model, which is $\Gamma_c \propto H^{-1}$ for $\sqrt{\eta_r}/H < 1$, as shown in Fig. 4(b). At higher values of $\sqrt{\eta_r}/H$, there is no instability, similar to the case of a linear elastic solid [6].

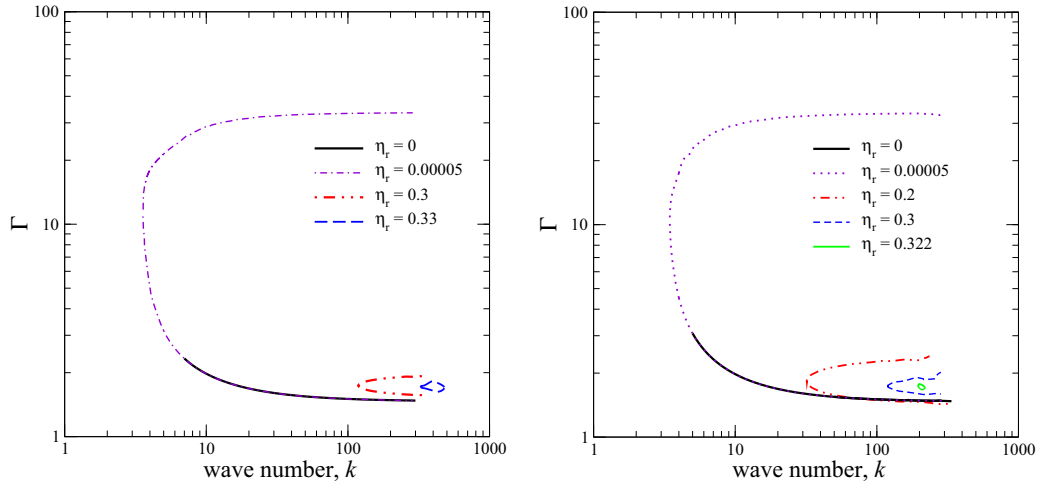

FIG. 5. Pressure-driven flow in a channel with deformable walls in the creeping-flow limit and the effect of the solid-fluid viscosity ratio η_r on the neutral stability curves for (a) $H = 0.5$ and (b) $H = 1$. The short-wave instability is stabilized with an increase in η_r and the instability eventually disappears after a critical η_r.

B. Channel flow

We next discuss the role of dissipation in the solid for the case of pressure-driven flow in a neo-Hookean channel, with the rate-of-deformation formulation being used for the dissipative part of stresses in the solid. For flow in a channel with deformable walls, there are two possible types of modes, viz., sinuous and varicose modes of deformation of the two channel walls. The work of Gaurav and Shankar [9] showed that, in contrast to Couette flow, there is no finite-wave-mode instability in the channel flow in the creeping-flow limit for a pure elastic neo-Hookean solid, but there is a short-wave instability that exists for all thicknesses. Because of the small length scales associated with the short-wave instability, the critical Γ for this mode is unaffected by the nature of the symmetry conditions (viz., sinuous or varicose) used at the channel center line. Hence, our results for the short-wave instability for nonzero values of η_r are similarly unaffected by the centerline boundary conditions. With the inclusion of viscosity of the solid, the neutral curve for the short-wave mode turns back in the Γ-k plane, and upon further increment in viscosity, the region of the short-wave instability shrinks in size in the Γ-k plane and the instability eventually disappears. Thus, the short-wave mode gets fully stabilized after a critical value of viscosity (see Fig. 5) similar to the case of Couette flow [Fig. 2(b)]. Our results thus indicate that beyond a critical value of η_r, there is no instability in the creeping-flow regime for pressure-driven flow in a deformable channel.

V. CONCLUSION

Linear stability analysis is carried out for the case of plane Couette flow past a deformable neo-Hookean solid in the creeping-flow limit using two different formulations for incorporating dissipative effects in the solid. One formulation proposes that the dissipative part of stress is proportional to the strain-rate tensor based on the left Cauchy-Green deformation tensor [22], while the other postulates that the dissipative stress is proportional to the rate-of-deformation tensor $\mathbf{D}$ [25]. However, the formulation involving the strain-rate tensor violates the fundamental principle of material-frame indifference in continuum mechanics [25] and hence cannot be a valid candidate for modeling dissipative effects in the solid. Nonetheless, some previous studies [22,23] have used this formulation to analyze the stability of fluid flow past deformable solid surfaces. In the present study, we used both formulations for the dissipative stress and we have shown that the results for the stability of the plane Couette flow are drastically different. For a pure elastic solid, the neutral curves in the Γ-k plane show the existence of both short-wave and finite-wave modes. For $H \leqslant 1$, the short-wave mode is critical for the instability and the finite-wave mode is critical for $H \geqslant 2$. With the inclusion of solid viscosity, both models give drastically different results and the salient differences are summarized below.

The formulation involving the strain-rate tensor yields the following results.

(i) At low values of H (<1), an increase in viscosity has the opposite effect on the short-wave mode (stabilizing) and the finite-wave mode (destabilizing) and there is a switch in the critical mode at $\eta_r = 0.5$. For $\eta_r < 0.5$, the short-wave mode is critical, while for $\eta_r > 0.5$, the finite-wave mode is critical.

(ii) At low values of H (<1), the short-wave mode is completely stabilized at $\eta_r \approx 1$.

(iii) At high H (>1), the finite-wave mode is the most critical for instability, but the Γ_c (critical strain rate) for this finite-wave mode is higher than that obtained for a purely elastic solid, thus indicating a stabilizing action of solid viscosity.

(iv) For nonzero solid viscosity and $H > 1$, two different scalings are observed (as reported in [22]), one in the regime of $H < \sqrt{\eta_r}$, with $\Gamma_c \propto H^{-1}$, and the other in the regime of $H > \sqrt{\eta_r}$, with $\Gamma_c \propto H^{-1/2}$. However, the actual value of Γ_c is higher than that obtained for a purely elastic solid for $H < \sqrt{\eta_r}$, while Γ_c is lower than that for a purely elastic solid for $H > \sqrt{\eta_r}$.

In contrast, the following are the corresponding results obtained for the rate-of-deformation tensor $\mathbf{D}$.

(i) At low H (<1), there exists an upper bound in the Γ-k plane for the short-wave mode, while the upper bound is absent in the strain-rate formulation. With an increase in viscosity η_r, the finite-wave and short-wave modes merge, but again separate into distinct modes for $\eta_r = 0.33$.

(ii) The unstable region for the short-wave mode forms a closed curve in the Γ-k plane, whose size shrinks with an increase in η_r. The short-wave mode is completely stabilized at $\eta_r > 0.35$.

(iii) In contrast, at low H, the finite-wave instability gets destabilized by an increase in η_r, compared to the case of a purely elastic neo-Hookean solid.

(iv) At high H (>1), the finite-wave mode is critical for instability, but the Γ_c (critical strain rate) is higher than that compared to the value obtained for a pure elastic solid. This trend is similar to the one obtained using the strain-rate formulation.

(v) There exists no instability for solid thickness values between $H = 1.21$ and 1.46 when $\eta_r = 1$. This behavior is absent in the strain-rate-tensor formulation. However, for the case of $\eta_r = 0.3$, instability exists at all H.

(vi) For nonzero solid viscosity and $H > 1$, the formulation using the rate-of-deformation tensor exhibits only one scaling behavior in the regime of $H < \sqrt{\eta_r}$, with $\Gamma_c \propto H^{-1}$, which is the same as the prediction obtained from the linear elastic solid [6].

Thus, the present study shows that the predictions for stability of flow past deformable solid media are sensitively dependent on the formulation employed to model dissipative stresses in the solid. This is especially important for solid thickness $H < 1$, where the consistent formulation using the rate-of-deformation tensor predicts that the role of viscosity in the solid can be destabilizing compared to a purely elastic neo-Hookean solid. We further showed that an increase in the solid viscosity leads to a complete stabilization of the short-wave instability (driven by the first normal stress difference in the solid) and the finite-wave mode becomes the most critical mode. For the case of pressure-driven flow in a deformable channel, our results show that there is no finite-wave instability at any value of η_r. The short-wave instability is fully suppressed when η_r increases beyond a critical value, very similar to the plane Couette flow case. These predictions will have important bearing on the comparison of theoretical and experimental studies in the stability of flow past soft solid surfaces.

ACKNOWLEDGMENTS

We thank Dr. Anurag Gupta, Department of Mechanical Engineering, IIT Kanpur, for instructive discussions in continuum mechanics. We also thank the anonymous referee for instructive comments.

APPENDIX

The governing equations using the strain-rate tensor $\dot{\mathbf{E}}$ for viscous dissipation are given below [22]. The nondimensional shear stress in the solid $\boldsymbol{\sigma}$ is of the form

$$\boldsymbol{\sigma} = -p_s\mathbf{I} + 2\mathbf{E}_{\text{left}} + 2\eta_r\dot{\mathbf{E}}_{\text{left}}, \tag{A1}$$

where $\mathbf{E}_{\text{left}} = \frac{1}{2}(\mathbf{F}\cdot\mathbf{F}^T - \mathbf{I})$ and $\dot{\mathbf{E}}_{\text{left}} = \frac{1}{2}\frac{\partial}{\partial t}(\mathbf{F}\cdot\mathbf{F}^T - \mathbf{I})$. The governing equations of the fluid are

$$d_z\tilde{v}_z + ik\tilde{v}_x = 0, \tag{A2}$$

$$-ik\tilde{p}_f + \left(d_z^2 - k^2\right)\tilde{v}_x = 0, \tag{A3}$$

$$-d_z\tilde{p}_f + \left(d_z^2 - k^2\right)\tilde{v}_z = 0. \tag{A4}$$

The linearized equations governing the solid are

$$d_{X_3}\tilde{x}_3 + ik\tilde{x}_1 - ik\Gamma\tilde{x}_3 = 0, \tag{A5}$$

$$-ik\tilde{p}_s + (1 + s\eta_r)\left(d_{X_3}^2 - k^2\right)\tilde{x}_1 = 0, \tag{A6}$$

$$ik\Gamma\tilde{p}_s - d_{X_3}\tilde{p}_s + (1 + s\eta_r)\left(d_{X_3}^2 - k^2\right)\tilde{x}_3 = 0. \tag{A7}$$

The linearized boundary conditions at the fluid-solid interface are given by

$$\tilde{v}_x + \Gamma\tilde{x}_3 - s\tilde{x}_1 = 0, \tag{A8}$$

$$\tilde{v}_z - s\tilde{x}_3 = 0, \tag{A9}$$

$$ik\Gamma^2\tilde{x}_3 - (1+s\eta_r)[ik\tilde{x}_3 + d_{X3}\tilde{x}_1 + \Gamma d_{X3}\tilde{x}_3] + d_z\tilde{v}_x + ik\tilde{v}_z = 0, \tag{A10}$$

$$\tilde{p}_s - 2(1+s\eta_r)d_{X3}\tilde{x}_3 - \tilde{p}_f + 2d_z\tilde{v}_z - k^2\gamma\tilde{x}_3 = 0. \tag{A11}$$

Analytical solutions of the fluid and solid governing equations are obtained as

$$\tilde{v}_z(z) = A_1e^{-kz} + A_2ze^{-kz} + A_3e^{kz} + A_4ze^{kz}, \tag{A12}$$

$$\tilde{x}_3(z) = B_1e^{-kz} + B_2e^{(-1+i\Gamma)kz} + B_3e^{-kz} + B_4e^{(1+i\Gamma)kz}. \tag{A13}$$

[1] G. M. Whitesides, The origins and the future of microfluidics, Nature (London) **442**, 368 (2006).

[2] A. D. Stroock, S. K. W. Dertinger, A. Ajdari, I. Mezić, H. A. Stone, and G. M. Whitesides, Chaotic mixer for microchannels, Science **295**, 647 (2002).

[3] A. D. Stroock, S. K. W. Dertinger, G. M. Whitesides, and A. Ajdari, Patterning flows using grooved surfaces, Anal. Chem. **74**, 5306 (2002).

[4] V. Hessel, H. Löwe, and F. Schönfeld, Micromixers—A review on passive and active mixing principles, Chem. Eng. Sci. **60**, 2479 (2005).

[5] T. M. Squires and S. R. Quake, Microfluidics: Fluid physics at the nanoliter scale, Rev. Mod. Phys. **77**, 977 (2005).

[6] V. Kumaran, G. H. Fredrickson, and P. Pincus, Flow induced instability of the interface between a fluid and a gel at low Reynolds number, J. Phys. France II **4**, 893 (1994).

[7] V. Kumaran and R. Muralikrishnan, Spontaneous Growth of Fluctuations in the Viscous Flow of a Fluid Past a Soft Interface, Phys. Rev. Lett. **84**, 3310 (2000).

[8] V. Gkanis and S. Kumar, Instability of creeping Couette flow past a neo-Hookean solid, Phys. Fluids **15**, 2864 (2003).

[9] Gaurav and V. Shankar, Stability of pressure-driven flow in a deformable neo-Hookean channel, J. Fluid Mech. **659**, 318 (2010).

[10] Gaurav and V. Shankar, Stability of fluid flow through deformable neo-Hookean tubes, J. Fluid Mech. **627**, 291 (2009).

[11] A. Shrivastava, E. L. Cussler, and S. Kumar, Mass transfer enhancement due to a soft elastic boundary, Chem. Eng. Sci. **63**, 4302 (2008).

[12] C. Yang, C. A. Grattoni, A. H. Muggeridge, and R. W. Zimmerman, A model for steady laminar flow through a deformable gel-coated channel, J. Colloid Interface Sci. **226**, 105 (2000).

[13] M. Gad-el-Hak, in *IUTAM Symposium on Flow Past Highly Compliant Boundaries and in Collapsible Tubes*, edited by P. W. Carpenter and T. J. Pedley (Kluwer Academic, Dordrecht, 2003), Chap. 9, p. 191.

[14] P. Krindel and A. Silberberg, Flow through gel-walled tubes, J. Colloid Interface Sci. **71**, 39 (1979).

[15] M. K. S. Verma and V. Kumaran, A multifold reduction in the transition Reynolds number, and ultra-fast mixing, in a micro-channel due to a dynamical instability induced by a soft wall, J. Fluid Mech. **727**, 407 (2013).

[16] S. S. Srinivas and V. Kumaran, After transition in a soft-walled microchannel, J. Fluid Mech. **780**, 649 (2015).

[17] R. Muralikrishnan and V. Kumaran, Experimental study of the instability of viscous flow past a flexible surface, Phys. Fluids **14**, 775 (2002).
[18] M. D. Eggert and S. Kumar, Observations of instability, hysteresis, and oscillation in low-Reynolds number flow past polymer gels, J. Colloid Interface Sci. **278**, 234 (2004).
[19] V. Shankar and V. Kumaran, Weakly nonlinear stability of viscous flow past a flexible surface, J. Fluid Mech. **434**, 337 (2001).
[20] R. Neelamegam, D. Giribabu, and V. Shankar, Instability of viscous flow over a deformable two-layered gel: Experiment and theory, Phys. Rev. E **90**, 043004 (2014).
[21] M. K. S. Verma and V. Kumaran, A dynamical instability due to fluid-wall coupling lowers the transition Reynolds number in the flow through a flexible tube, J. Fluid Mech. **705**, 322 (2012).
[22] P. Chokshi and V. Kumaran, Weakly nonlinear analysis of viscous instability in flow past a neo-Hookean surface, Phys. Rev. E **77**, 056303 (2008).
[23] P. Choskshi and V. Kumaran, Stability of the flow of a viscoelastic fluid past a deformable surface in the low Reynolds number limit, Phys. Fluids **19**, 104103 (2007).
[24] M. Destrade, G. Saccomandi, and M. Vianello, Proper formulation of viscous dissipation for non-linear waves in solids, J. Acoust. Soc. Am. **133**, 1255 (2013).
[25] L. E. Malvern, *Introduction to the Mechanics of a Continuous Medium* (Prentice-Hall, Englewood Cliffs, 1969).
[26] G. A. Holzapfel, *Nonlinear Solid Mechanics* (Wiley, Chichester, 2000).
[27] M. Destarde and G. Saccomandi, Finite-amplitude inhomogeneous waves in Mooney-Rivlin viscoelastic solids, Wave Motion **40**, 251 (2004).
[28] N. Phan-Thien, Squeezing flow of a viscoelastic solid, J. Non-Newtonian Fluid Mech. **95**, 343 (2000).
[29] K. Hashiguchi, *Elastoplasticity Theory* (Springer, Berlin, 2013).
[30] S. S. Antman, Physically unacceptable viscous stresses, Z. Angew. Math. Phys. **49**, 980 (1998).
[31] Y. Z. Wang, H.-H. Dai, and W. Q. Chen, Kink and kink-like wave in pre-stretched Mooney-Rivlin viscoelastic rods, AIP Adv. **5**, 087167 (2015).
[32] J. A. Weideman and S. C. Reddy, A Matlab differentiation matrix suite, ACM Trans. Math. Software **26**, 465 (2000).